Computational and Structural Biotechnology Journal 19 (2021) 2938–2949

COMPUTATIONAL AND STRUCTURAL BIOTECHNOLOGY JOURNAL

journal homepage: www.elsevier.com/locate/csbj

Endogenous modulators of neurotrophin signaling: Landscape of the transient ATP-NGF interactions

Francesca Paoletti [a,*], Franci Merzel [a], Alberto Cassetta [b], Iza Ogris [a], Sonia Covaceuszach [b], Jože Grdadolnik [a], Doriano Lamba [b,c], Simona Golič Grdadolnik [a,*]

[a] Laboratory for Molecular Structural Dynamics, Theory Department, National Institute of Chemistry, Hajdrihova 19, SI-1001 Ljubljana, Slovenia
[b] Institute of Crystallography – C.N.R.– Trieste Outstation. Area Science Park – Basovizza, S.S.14 – Km. 163.5, I-34149 Trieste, Italy
[c] Interuniversity Consortium "Biostructures and Biosystems National Institute", Viale delle Medaglie d'Oro 305, I-00136 Roma, Italy

ARTICLE INFO

Article history:
Received 23 February 2021
Received in revised form 29 April 2021
Accepted 2 May 2021
Available online 07 May 2021

Keywords:
Neurotrophins
Endogenous ligands
ATP modulation
TrkA, p75^{NTR} receptors
NGF interactions

ABSTRACT

The Nerve Growth Factor (NGF) neurotrophin acts in the maintenance and growth of neuronal populations. Despite the detailed knowledge of NGF's role in neuron physiology, the structural and mechanistic determinants of NGF bioactivity modulated by essential endogenous ligands are still lacking. We present the results of an integrated structural and advanced computational approach to characterize the extracellular ATP-NGF interaction. We mapped by NMR the interacting surface and ATP orientation on NGF and revealed the functional role of this interaction in the binding to TrkA and p75^{NTR} receptors by SPR. The role of divalent ions was explored in conjunction with ATP. Our results pinpoint ATP as a likely transient molecular modulator of NGF signaling, in health and disease states.

1. Introduction

The NGF is the first discovered member of the NT family [1]. It is essential for the development and phenotypic maintenance of neurons in central and peripheral nervous systems. It has a crucial role in activation of the immune and endocrine systems and in the pain pathway [2]. Mature NGF is obtained by furin protease cleavage from the precursor proNGF [3]. NGF binds with high affinity to the tyrosine kinase TrkA receptor, determining cell survival and differentiation, as well as to p75^{NTR} receptor triggering apoptosis [4,5]. proNGF creates a signaling complex by simultaneously interacting with p75^{NTR} and a member of the family of Vps10p-domain receptors, Sortilin [6].

Translational and clinical research highlighted the spectrum of diseases that could benefit from NGF treatment (*e.g.* Alzheimer's Disease, diabetic skin wound healing, corneal pathologies, etc.) [7]. Its therapeutic application has been limited owing to poor plasma stability, restricted nervous system penetration and, importantly, the pleiotropic actions deriving from its concomitant binding to multiple receptors. One strategy to overcome these limitations is to target NGF and/or individual NGF receptors with small molecule ligands. The latter might also modulate various aspects of the involved signaling pathways in distinct ways from the native NTs. These ligands might provide novel therapeutic options for a broad range of neurological indications [2,8–12].

There are very few reports, which explored the role of essential endogenous ligands as modulators of NGF biological activity [13–19]. The ability of DNA, RNA, oligonucleotides, lipids and glycosaminoglycans to gate the facilitatory action of NGF on its signaling pathways has been seldom considered [13–19]. Thus, a deeper understanding of the molecular determinants of the ligands

Abbreviations: ARIA, Ambiguous Restraints for Iterative Assignment; BDNF, Brain Derived Neurotrophic Factor; CARA, Computer Aided Resonance Assignment; CS-E, Chrondroitin Sulfate E; CSP, Chemical Shift Perturbation; DSF, Differential Scanning Fluorimetry; EI-MS, Electron Ionization Mass Spectrometry; FGF2, Fibroblast Growth Factor 2; FT-IR, Fourier Transform Infrared Spectroscopy; HBD, Heparin Binding Domain; HSQC, Heteronuclear Single Quantum Coherence; ITC, Isothermal Titration Calorimetry; MALDI-TOF MS, Matrix Assisted Laser Desorption Ionization-Time Of Flight Mass Spectrometry; MD, Molecular Dynamics; MS, Mass Spectrometry; NGF, Nerve Growth Factor; NMR, Nuclear Magnetic Resonance; NOE, Nuclear Overhouser Effect; NOESY, Nuclear Overhauser Effect Spectroscopy; NT, NeuroTrophin; P20, Polysorbate 20; p75^{NTR}, p75 NeuroTrophin Receptor; PME, Particle Mesh Ewald; proNGF, proNGF – NGF precursor; rhNGF, recombinant human NGF; rh-proNGF, recombinant human proNGF – NGF precursor; rmNGF, recombinant mouse NGF; RMSD, Root Mean Square Deviation; SAR, Structure-Activity Relationship; SPR, Surface Plasmon Resonance; STD, Saturation-Transfer Difference; TrkA, Tyrosine Kinase Receptor A.

* Corresponding authors.
E-mail addresses: francesca.paoletti@ki.si (F. Paoletti), simona.grdadolnik@ki.si (S. Golič Grdadolnik).

https://doi.org/10.1016/j.csbj.2021.05.009

binding mode is required to better appreciate and potentially exploit the therapeutic potential of NGF.

Recently, ATP binding has been reported for protein families, which lack the ATP-binding domain. It has been proven that NGF binds to ATP and that the formed complex protects hippocampal neural cells from death [20–23]. The ligand signature and the physiological role of the extracellular ATP-NGF interrelationship remain however to be elucidated [21,22]. Similar observations were reported for another member of the NT family, BDNF [24], as well as for other growth factors (FGF [25], Vascular Endothelial Growth Factor [26]). The ATP-NGF association and the role of the concomitant presence of divalent ions have been analyzed by MS [21]. It was suggested by analogy to other ATP-binding proteins that ATP might bind NGF at a putative heparin-binding site [22].

ATP metabolism, in different cellular contexts, is regulated by divalent cations, among which, the role of Mg^{2+} and Zn^{2+} is of particular interest [27–29]. Zn^{2+} binding is characterized by a tightly regulated homeostasis and its link to cytotoxicity has been proven [27–29]. Zn^{2+} interaction with NTs has been reported [30,31].

It is well known that the release of ATP into the brain is finely tuned [32,33]. Different extracellular ATP levels in brain have been detected in health or disease conditions, and related to the activation of specific subclasses of P2 receptors [32,33]. A set of crucial cellular studies, investigating the ATP neurotrophic role in synergy with NGF highlighted a crosstalk between neurotrophins signaling and the purinergic receptors system, in different disease states [34,35]. The relative extracellular levels of ATP and NGF were reported to be involved in the interaction with their specific receptors. The unbalance in the extracellular levels of both ATP and NGF would be a key factor into the cellular response to cell damage. ATP was reported to have a role into PC12 cells activation, synergistically with NGF [35]. However, the lack of knowledge on the structural determinants and of the thermodynamic fingerprints of the ATP-NGF interactions, represent a major drawback towards the understanding of the underlying functional and biological properties of the complex.

We carried out a thorough structural/biophysical study including state-of-the-art solution NMR, integrated by extensive MD simulations aimed at investigating the interaction of ATP with rhNGF**.** For the characterization of ATP-rhNGF binding, we used 2D HSQC experiments, the most robust NMR method for detecting and evaluating weak ligand–protein binding. This technique, was originally exploited for detecting weak small fragments binders to protein targets by using the so-called SAR by NMR approach [36]. Since then it is one of the most important fragment screening methods, not only because of its sensitivity in detecting weak interactions (K_D in the μM to mM range), but also it is frequently used as validation tool to confirm specific binding [37–39]. The cartography of the interactions between ATP and rhNGF unveiled the binding sites on the molecular surface and the ligand's orientation. An SPR analysis allowed investigating the functional role of this interaction in the context of TrkA and $p75^{NTR}$ receptors. The functional role of divalent ions in conjunction with ATP was also exploited. The present structural analysis pinpoints ATP as a genuine endogenous modulator of NGF signaling *in vivo*, in health and disease conditions.

2. Materials and methods

2.1. Expression, refolding and purification of rhNGF

rhNGF was recombinantly expressed according to well established protocols which exploit the *in vitro* refolding and subsequent proteolytic cleavage from its precursor rh-proNGF. rhNGF was expressed in Rosetta (DE3) *E. Coli* cells, transformed with the pET11a plasmid containing the cDNA of human proNGF VSAR . The mutation RSKR – VSAR at furin cleavage site allowed the introduction of a specific trypsin cleavage for the preparation of mature rhNGF (US Patent 2015/0087020). Solubilization and refolding of rh-proNGF from inclusion bodies was carried out according to published protocols [40]. Mature rhNGF was obtained by controlled trypsin cleavage of rh-proNGF [41]. Optimization of the expression of rh-proNGF VSAR in minimal medium with ^{15}N- or ^{15}N-^{13}C labeling was needed, starting from the conditions described for the recombinant mouse proNGF [41]. The best expression conditions were obtained by supplementing M9 medium with 0.4% glucose and upon induction with IPTG for 18 h at 25 °C. The integrity of rhNGF was confirmed by MALDI-MS analysis. Protein fold was characterized by biophysical techniques (DSF, FT-IR, NMR).

2.2. NMR experiments

The high-resolution spectra were recorded on Agilent Technologies DD2 600 MHz and VNMRS 800 MHz Spectrometers, using cryoprobes, at 30 °C.

2.2.1. NMR experiments for rhNGF spectral assignment

The HNCA, ^{15}N NOESY-HSQC, ^{13}C NOESY-HSQC spectra were acquired at 800 MHz on samples containing ^{15}N- or ^{15}N, ^{13}C-labelled rhNGF (0.1 mM) in 50 mM Hepes at pH 7 and 10% D_2O. HNCA experiment was employed to obtain sequence specific $^{13}C_\alpha$ backbone assignments [42]. ^{15}N NOESY-HSQC, ^{13}C NOESY-HSQC were used for side chain aliphatic assignments. All spectra were processed using NMRPipe/NMR-Draw [43] and analyzed using CARA [44]. Intra-molecular proton distance restraints were derived from ^{15}N- and ^{13}C-NOESY-HSQC spectra (mixing time 100 ms). Backbone assignment was guided by the identification of the expected set of connectivities within and inter-strands, while side chains assignment was complicated by the severe overlap of resonances from highly abundant Leu, Ile, Lys, Arg residues. Backbone and side chain assignment was completed at 82% and 74%, respectively, and deposited in the BMRB database (ID: 34515).

2.2.2. Structure determination of rhNGF

Automated NOESY cross-peak assignments and structure determination were performed using ARIA 2.3 software [45,46]. The NMR structural bundle was generated by ARIA using as input the ambiguous and unambiguous intra-protomer NOE distance restraints (both manually and automatically assigned) derived from ^{15}N- and ^{13}C-NOESY-HSQC aliphatic experiments at 30 °C, in addition to a set of manually assigned unambiguous inter-protomer restraints. The total number of unambiguous restraints used in the calculations was 1584 (per protomer), of which 1528 intramolecular and 56 intermolecular. Structure-derived H-bonds (25/protomer) were also used as restraints, the latter only being introduced when present in 50% of the preliminary calculations. In the final ARIA run, 200 structures were generated in the last iteration. After refinement of the 60 lowest global energy structures by MD simulation with explicit water, 20 structures ranked on global energy were selected as representative of the structure and used for statistical analysis. Structure quality was evaluated with PROCHECK at the final stage of the calculations by ARIA. The ensemble obtained at the end of the refinement process converged, with an average RMSD of 1.05 Å from the medoid structure as calculated on residues with a well-defined secondary structure (16–22; 27–30; 33–37; 41–44; 47–50; 53–58; 77–91; 98–113). The coordinates of the rhNGF structure are deposited in the PDB (ID: 6YW8).

2.2.3. NMR experiments for determination of ATP-rhNGF binding

The ^1H STD experiments were recorded at 600 MHz on samples containing unlabeled rhNGF at 20 μM prepared in 50 mM Tris-d_{11}

and 50 mM NaCl in D_2O, pD 7.3 buffer. The residual water was suppressed using excitation sculpting with 5 ms selective pulse. $T_1\rho$ filter of 30 ms was used to eliminate the background protein resonances. The STD spectra were recorded at a ATP-rhNGF ratio of 100:1. To achieve the excess of the cations (50-fold for Mg^{2+} or 25-fold for Zn^{2+}), 1 mM $MgCl_2$ or 0.25 mM $ZnCl_2$ were added to the samples, with a protein concentration of 20 μM (sample with Mg^{2+}) or 10 μM (sample with Zn^{2+}). Notably, the presence of Zn^{2+} required strict controlling of the experimental conditions. Zn^{2+} itself affects the sample, resulting in protein precipitation outside an optimized ATP- Zn^{2+}-rhNGF stoichiometric ratio.

The ^1H STD ligand epitope mapping experiments [47] were performed under quantitative conditions considering the nonuniform relaxation properties of ATP. The inversion recovery T_1 experiments showed that the ^1H T_1 relaxation times of ATP range from 3.9 s in the adenine moiety to 0.43 s in the sugar moiety. Therefore STD amplification factors were determined with a short saturation delay of 0.21 s to avoid the effect of the longitudinal relaxation rate on the signal intensities [48]. Spectra were recorded with a 6578 Hz spectral width, 16,384 data points, a relaxation delay of 5 s and 4500–10600 scans. Selective saturation was achieved by a train of 50 ms long Gauss-shaped pulses separated by 1 ms delay. The on-resonance selective saturation of rhNGF was applied at 0.32 ppm at transmitter offset referenced to 4.64 ppm. The off-resonance irradiation was applied at 30 ppm for the reference spectrum. Subtraction of the on and off-resonance spectra was performed internally *via* phase cycling. Spectra were zero-filled twice and apodized by an exponential line-broadening function of 3 Hz. Errors in the STD amplification factor were estimated according to the formula: STD amplification factor absolute error = STD amplification factor × $((N_{STD}/I_{STD})^2 + (N_{REF}/I_{REF})^2)^{1/2}$ [49]. N_{STD} and N_{REF} are noise levels in STD and reference spectra, respectively. I_{STD} and I_{REF} are signal intensities in STD and reference spectra, respectively.

2D ^1H-^{15}N HSQC spectra were recorded at 800 MHz spectra, with 1024 data points in t_2, 48 scans, 92 complex points in t_1 and a relaxation delay of 1.5 s. The ^1H and ^{15}N sweep widths were 11,161 and 2269 Hz, respectively. Samples contained ^{15}N labelled rhNGF (0.08 mM) in 50 mM Hepes at pH 7, 50 mM NaCl, 1 mM $MgCl_2$ and 10% D_2O. ATP stock solution was prepared in the same rhNGF buffer at 100 mM concentration, pH was carefully adjusted. For the titration experiment, subsequent ATP addition to the rhNGF were performed, according to the following list: rhNGF:ATP = 1:1; 1:2; 1:5; 1:10; 1:15; 1:20. The absence of ATP hydrolysis during the titration experiment was monitored by checking H2 and H8 protons resonance in ^1H NMR spectrum. At the titration endpoint (rhNGF:ATP = 1:20), the ^1H-^{15}N NOESY-HSQC spectrum was collected. All spectra were processed using NMRPipe/NMRDraw [43] and analyzed using CARA [44]. The combined $^1H/^{15}N$ CSP (Δδ) were calculated from ^1H and ^{15}N CSP using the equation: $\Delta\delta = ((\Delta\delta\ ^1H)^2 + (0.04 \times \Delta\delta\ ^{15}N)^2)^{1/2}$ [50].

2.3. DSF

DSF experiments were performed in triplicate using a CFX96 Touch Biorad real-time PCR instrument (Bio-Rad). rhNGF (0.5 mg/mL) in 50 mM Hepes, 150 mM NaCl pH 7.2 was pre-incubated with ATP and/or $ZnCl_2$ or $MgCl_2$ (0.1 mM) for 30 min at 4 °C before adding SYPRO orange dye (Sigma) at a final concentration of 90x. The fluorescence was measured as a function of increasing temperature in the 20°–90 °C range at the rate of 0.2 °C/min (excitation wavelength: 470–505 nm; emission wavelength: 540–700 nm). Melting temperatures (T_m) were obtained by fitting the sigmoidal melting curves to the Boltzmann equation [51].

2.4. FT-IR

The infrared spectra were recorded with a FT-IR Bruker Vertex 80 spectrometers with a nominal resolution of 2 cm^{-1} and an averaging of 128 scans and apodized with a Blackman-Harris 3-term function. All spectra were recorded at 25 °C with a Golden Gate ATR temperature-controlled cell (Specac). rhNGF at 0.15 mM concentration in 50 mM Hepes buffer, pH 7 was used. The visibility of the amide I and amide II bands was achieved by subtracting the original protein solution spectra with the spectrum of the Hepes buffer alone.

2.5. ITC

ITC experiments were carried out using an ITC 200 microcalorimeter (Malvern Panalytical, UK). Experiments were performed in 50 mM Hepes pH 7.2. rhNGF concentration was determined using a NanoDrop LITE Spectrophotometer (Thermo Fisher Scientific, US). 100 mM ATP stock solution was prepared in the same buffer. Both rhNGF and ATP samples were centrifuged for 5 min at 13000 rpm and degassed. Titrations were performed at 30.0° ± 0.1 °C with a stirring of 750 rpm to ensure rapid mixing. A first set of 19 injections of 2 μL, 2 mM ATP, were performed into a measurement cell filled with 200 μL of 40 μM dimeric rhNGF. The first set of titrations was followed by a set of 19 injections of ATP at the same concentration, to approach the plateau, for a grand total of 38 injections. The two measurements files were merged by using the software *concat* (Malvern). The same protocol was repeated two more times with 5 mM ATP while keeping rhNGF at 40 μM, to ensure a larger ATP-rhNGF final molar ratio. Negative control titrations were performed by running a set of 19 injections of 2 or 5 mM ATP into the cell filled with buffer only. Negative controls allowed for the estimation of ATP dilution heats.

Integration of the raw thermograms has been done with the program NITPIC [52] that allowed for a precise and unbiased extraction of the heats from the experimental curves.

Global fitting of the three ATP-rhNGF titration experiments by nonlinear least squares was performed to analyze the ATP-rhNGF binding isotherms by means of SEDPHAT software [53]. Due to the complexity of the binding interaction, the fitting procedure has been carried out by assuming one ATP binding site per protomer of rhNGF, as previously reported by mass spectrometry in the absence of divalent cations [22]. The binding sites on the two protomers were assumed strictly symmetric, as suggested from NMR data.

2.6. MD Simulations and Analysis

All atom MD simulations were performed using NAMD [54] with the CHARMM36 [55] force field and TIP3P water model on GPU server. The PME method was used for electrostatics with a real space cutoff of 12 Å. All bonds involving hydrogen atoms were constrained to their equilibrium values with the SHAKE algorithm. An integration time step of 2 fs was used. Simulations were carried out in the NPT ensemble with p = 1 atm and T = 300 K using Nose-Hoover algorithm and Langevin piston pressure control. NMR structure rhNGF was modeled at pK_a = 7.0 without applying the two-fold symmetry relationship between the protomers. In order to obtain insight into dynamical fluctuations in apo-form of rmNGF and rhNGF, we evaluated average RMSD per residue from the two separate 300 ns MD simulations performed for both dimers which were solvated by the neutral aqueous solution enclosed in the simulation box of 80 × 72 × 72 $Å^3$. Neutrality was achieved by the addition of the proper number of Cl^- counter-ions to the simulation box. Next, four different models of ATP-rhNGF + Mg^{2+} complex were generated in which different ATP poses, selected according

to the information obtained from the NOE analysis, were taken into account. All models were solvated by 50 mM NaCl. Each system was simulated for 600 ns under the same conditions.

An algorithm was developed to detect the most stable poses of ATP in contact with rhNGF. When analyzing the distances between given ATP and rhNGF hydrogens, we first selected ATP poses where the distances between the hydrogen atoms were shorter than 4.5 Å. The search was further substantiated by calculating the duration of each continuous contact during the MD simulation. The final selection was made under the requirement of a contact duration of more than 10 ns.

To quantitatively assess binding preferences of ATP for Site1 or Site2 from MD simulations, the potential energy differences between bound, '_B', (to site1/2) and unbound, '_U', states of ATP were calculated. The internal (self-) energy of the ATP molecule, $E_{\_AA}$, and its interaction energy with the surroundings, which include protein and solvent molecules, $E_{\_AS}$, were considered according to the following formula:

$$\Delta E_{\_1/2} = < E_{\_AS\_B} + E_{\_AA\_B} >_{\_1/2} - < E_{\_AS\_U} + E_{\_AA\_U} > \quad (1)$$

Each average <> was taken over 2000 frames of MD trajectory pre-selected according to the position of ATP molecule relative to Site1/2 or its unbound state. Omitting the change in internal energy of protein and solvent in (1), which is estimated to be comparable for both sites, and neglecting the change in molecular volume, the difference $\Delta E_{\_1}$-$\Delta E_{\_2}$ can be called the relative binding enthalpy of ATP.

2.7. SPR

Experiments were performed with a Biacore T100 equipment (GE Healthcare, UK), equipped with Biacore T100 Control software 2.0.1. The amine coupling reaction was performed according to manufacturer's instructions (GE Healthcare, UK), on CM5 chips.

2.7.1. ATP-rhNGF interaction

rhNGF was dissolved in 10 mM Sodium Acetate pH 5.5 at 100 μg/mL and immobilized at 8700 RU surface concentration on CM5 chip. Due to the very low binding response of ATP on rhNGF when injected as analyte, several attempts were made to increase the binding, by changing association times, coupled with different flows. No improvement was observed.

2.7.2. Kinetics and affinity experiments

TrkA (R&D, TrkA Fc Chimera, 175-TK-050) and $p75^{NTR}$ (R&D, R/TNFRSF16 Fc Chimera, 367-NR-050) receptors extracellular domains were used as ligands, dissolved in 10 mM Sodium Acetate pH 5 at 20 μg/mL and immobilized at a 3600 RU (TrkA) and 2600 RU ($p75^{NTR}$) surface concentration on CM5 chip. The analyte proteins were injected in Hepes Buffer Saline (20 mM Hepes, 150 mM NaCl, 0.005% P20, pH 7.2), at a flow rate of 30 μL/min, 180 s association time and 600 s dissociation time. Samples for the kinetics measurements were prepared by 1:1 serial dilution, starting from a mixture of rhNGF 50 nM and/or Mg^{2+} 500 nM, Zn^{2+} 500 nM, ATP 500 nM. Concentration of rhNGF for the kinetic analysis was in the range 0.39 nM−12.5 nM. Six different concentrations obtained by 1:1 dilution have been used. Chip regeneration was performed with 10 μL of 10 mM NaOH. Every dataset was repeated 3 times. The measurement of rhNGF alone was only carried out once, being the resulting kinetic analysis in agreement with the previously reported literature data [56]. Data analysis was carried out using Biacore T100 Evaluation 2.0.1 and BIAevaluation 3.2 Softwares. A 1:1 Langmuir fitting model was assumed for the evaluation of the kinetic and equilibrium constants.

3. Results

3.1. 3D NMR structure of rhNGF in solution

Using NMR we determined the solution structure of unbound rhNGF required for our ATP binding studies. The 2D ^{1}H-^{15}N HSQC spectrum of rhNGF, showing a good spectral dispersion (Supp. Fig. S1) was assigned almost to completeness (BMRB: 34515). The NOEs obtained from the 3D ^{15}N- and ^{13}C-NOESY-HSQC spectra were used for the 3D structural model construction and validation (Fig. 1a, b – PDB: 6YW8; Supp. Table S1). The solution structure closely resembles those determined by X-ray crystallography for rhNGF-ligand complexes (PDB: 1WWW, 1SG1, 2IFG, 2IJ2, 4EDW, 4EDX, 4ZBN, 5JZ7), especially as to the topology of the Cys-knot, whereas it exhibits notable differences within the flexible loop regions (Fig. 1c).

Loop III (residues 60–67), which is missing in all the X-ray crystal structures of bound rhNGF, showed to be flexible also in the apo rhNGF in solution, where residues 60–67 are absent or weak in the 2D ^{15}N HSQC spectrum (Supp. Fig. S1). The presence of side-chain NOEs in the ^{13}C-NOESY-HSQC spectra, as well as the inter-residues NOEs in the ^{15}N-NOESY-HSQC spectrum, allowed to partially define this region (Fig. 1b). A wider-open conformation of Loop II (residues 39–48), if compared with the crystallographic structures has also been identified. Furthermore, in the present NMR structure of unbound rhNGF, the N-terminus is flexible and lacks a specific secondary structure propensity, whereas in the X-ray crystal structures of the rhNGF-TrkA complex, it is involved in the interacting surface and adopts a helicoidal conformation (Fig. 1c).

The conformational plasticity of the rhNGF solution structure was also exploited by MD simulations and compared to the only other solution structure of a NT, namely that of rmNGF (Fig. 2, Supp. Figs. S1, S2). The analysis of RMSDs per residue in MD highlights regions with higher conformational plasticity, like Loop II (residues 39–48) in rmNGF as compared to rhNGF (Fig. 2a, b). Indeed, an opening of Loop II has been reported [17,59] in small ligands binding to mNGF (PDB: 4EAX, 4XPJ) or NGF from cobra venom (PDB: 4EC7). Looking at the N-terminus, earlier solution NMR studies on rmNGF prompted to the propensity of the N-terminal residues (1–10) to adopt an helicoidal structure [41]. On the contrary, in rhNGF, the N-terminal residues are poorly defined (Supp. Fig. S2). This was further confirmed by the analysis of evolution, in the MD trajectories, of the intra H-bonds (NH···CO distances) formation engaging the N-terminal residues of either rh- or rmNGF (Fig. 2c–h). These observed differences well agree with previous experiments aimed at the thorough characterization of the biochemical and biophysical properties of m- and hNGFs [60].

3.2. ATP interaction with rhNGF

Hunting for the structural and functional characterization of new endogenous modulators of hNGF biological activity, we deeply investigated its binding properties to ATP. FT-IR measurements (Supp. Fig. S3) ruled out changes in the secondary structure of rhNGF due to the interaction with ATP. SPR, ITC and 1D ^{1}H STD NMR pinpoint to low affinity (mM range) ATP-rhNGF binding. ITC titration data (Supp. Fig. S4) returned a K_D of 1.38 mM. As early defined in the 80′ [61] and underlined in the recent literature, transient interactions with weak affinities in the mM range, also named "quinary interactions" [61] were often neglected due to technical challenges in the isolation of molecular complexes to be described [62–64]. Still, these transient and weak quinary interactions are important in specific subcellular compartments and in specific cellular states, for the regulation of dynamic biological processes needed for cell survival [62,65,66]. Therefore, our data prompt to

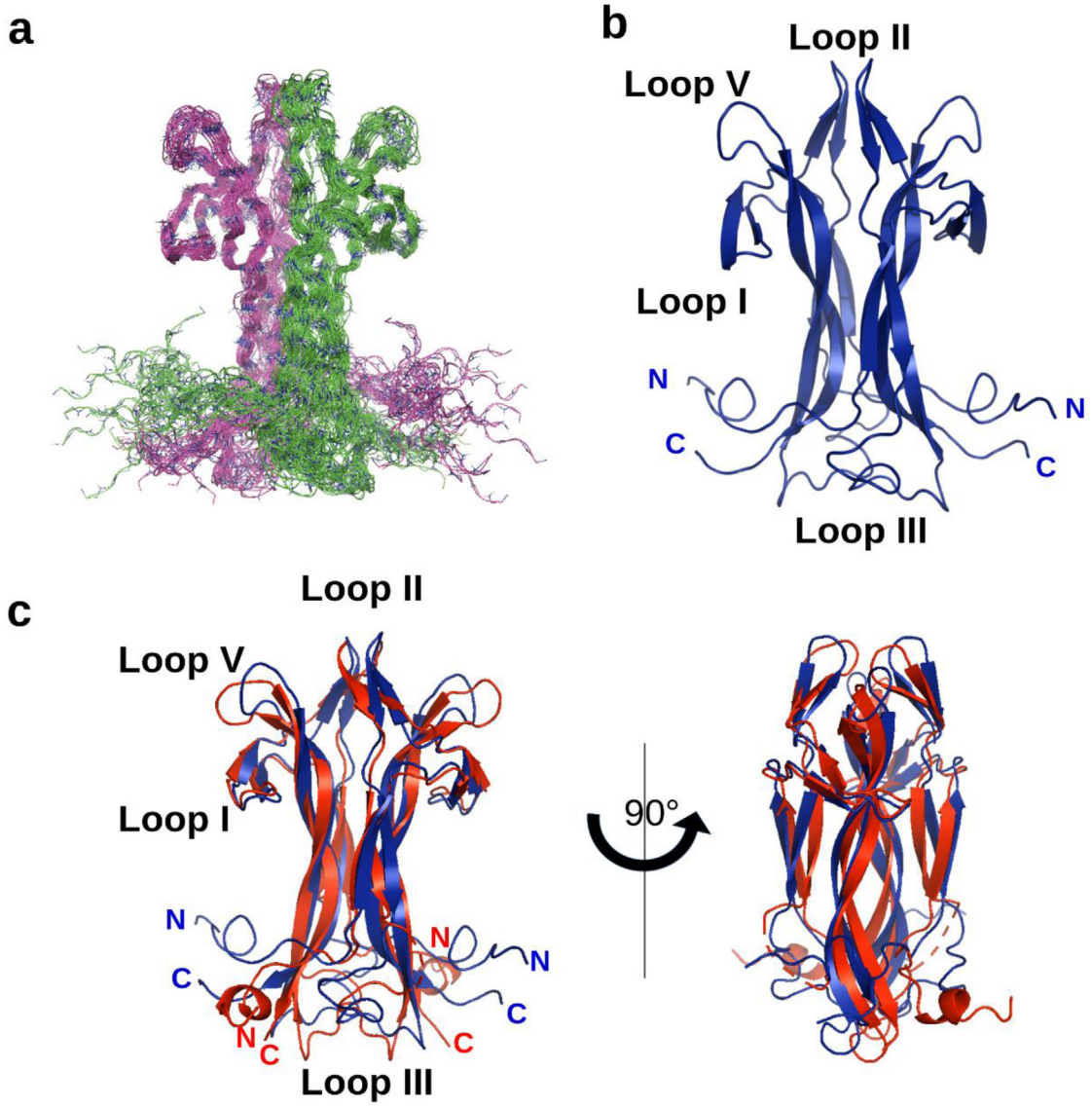

Fig. 1. 3D structure of rhNGF in solution. a) Overlay of the 20 lowest global energy models after ARIA refinement in explicit water. The protein backbone is shown as ribbon. The two protomers are colored in green and magenta, respectively. b) Cartoon model of the medoid solution NMR structure of rhNGF (PDB: 6YW8). c) Cartoon model of the medoid solution NMR structure of rhNGF (blue; PDB: 6YW8) superimposed with the X-ray crystal structure of rhNGF (red; PDB ID: 1WWW). Loops have been labelled according to MacDonald et al. [57]. Figure produced using PyMOL [58]. (For interpretation of the references to colour in this figure legend, the reader is referred to the web version of this article.)

ATP as a modulator of NTs activity. DSF explored the effects of different divalent cations on the binding interactions between ATP and rhNGF. A major effect of ATP on rhNGF thermal stability occurred in the presence of Zn^{2+} (Supp. Fig. S5). SPR analysis confirmed that ATP binding to rhNGF was markedly affected by Zn^{2+} (Supp. Fig. S6). 1D ^{1}H STD NMR experiments [47] were used to determine the binding epitope of ATP when bound to rhNGF in the presence of either Mg^{2+} or Zn^{2+} ions. In either case, the strongest interaction was observed for H2 on the adenine and H4' on the sugar moieties of ATP, respectively (Supp. Fig. S7). Our 1D ^{1}H STD NMR experiments complete and extend the previous MS findings by highlighting the ATP functional groups involved in the binding to rhNGF [22].

3.3. ATP-rhNGF binding: Identification of binding surface

2D ^{1}H-^{15}N HSQC spectra following a titration with increasing amounts of ATP (Supp. Fig. S8) allowed to characterize the rhNGF residues engaged in the interactions with ATP. The analysis of the combined ^{1}H/^{15}N CSP ($\Delta\delta$) showed residues that are likely involved directly in ATP binding with ^{1}H/^{15}N CSP ($\Delta\delta$) larger than 0.04 ppm (Fig. 3).

These residues, localized in Loops I, II and V showed to be clustered in close spatial proximity on the NMR solution structure of rhNGF (Supp. Fig. S9) and their close neighbors in space show a change in the NOE pattern, consistent with changes in their chemical environment due to the presence of ATP (Table 1, lower row). An earlier study [22] based on MS and mutagenesis studies reported the involvement of the C-terminus of rhNGF in ATP binding. Our data instead clearly show no involvement of this region in rhNGF binding. The 3D ^{15}N-NOESY-HSQC spectrum, collected at the titration endpoint, allowed the identification of definite newly originated NOEs upon ATP binding, which were unambiguously attributed to ATP protons (Table 1; Supp. Figure S10, Table S2). This analysis points towards the presence of two previously unknown binding sites for ATP on each rhNGF protomer, with a 4:2 (ATP:

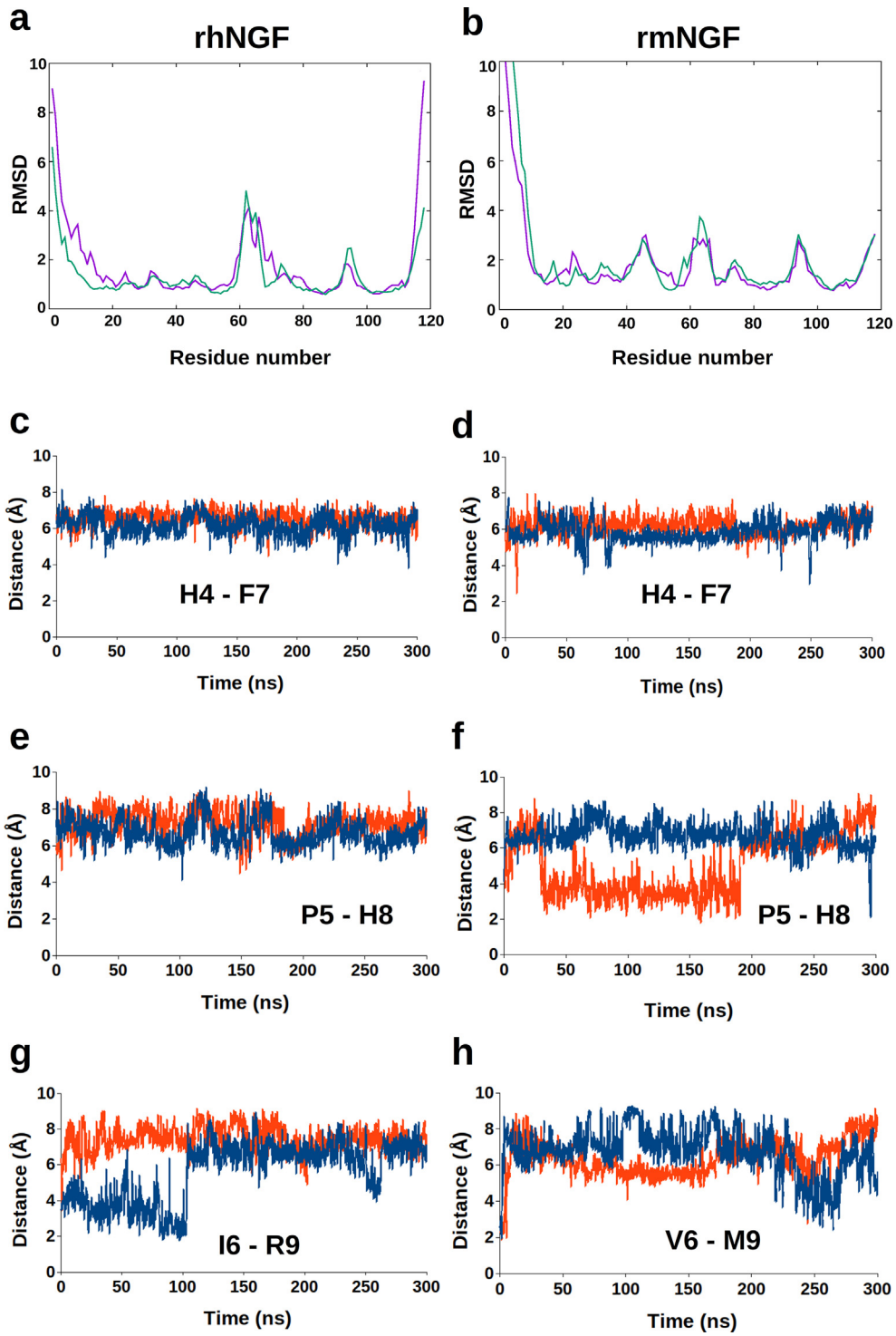

Fig. 2. Comparison of the 3D NMR solution structures of rhNGF and rmNGF: MD results. (a, b) RMSD per residue averaged over the 300 ns MD simulation of rhNGF (PDB: 6YW8) and rmNGF (PDB: 5LSD) *versus* residue position for the two protomers (purple—protomer 1; green—protomer 2). (c, d, e, f, g, h) MD Evolution of the distances (Å), along the 300 ns MD simulation, between atoms engaged in the hydrogen bonds that stabilize the helical structure of the N-terminus of rhNGF (c, e, g) or rmNGF (d, f, h) (blue—protomer 1; red—protomer 2). Atoms pairs analyzed are indicated on the panels. (For interpretation of the references to colour in this figure legend, the reader is referred to the web version of this article.)

rhNGF) stoichiometry. We named the site encompassing residues V20 and E55 as "Site 1" and that defined around F49 as "Site 2" (Table 1).

The new NOEs attributable to ATP were included to drive MD simulations aimed at mapping the likely binding orientation of ATP on rhNGF. During unbiased and constraint-free simulations of 2.4 μs, the ATP molecule was found migrating over few different protein sites without an expressed tendency to remain trapped in any specific pose.

In a subsequent analysis, we identified all ATP positions explored during MD simulations that correspond to a continuous contact between selected ATP and rhNGF hydrogens lasting longer than 10 ns. These poses are depicted in Fig. 4 (a, b). Interestingly, most of them nicely match the ATP binding sites resulting from

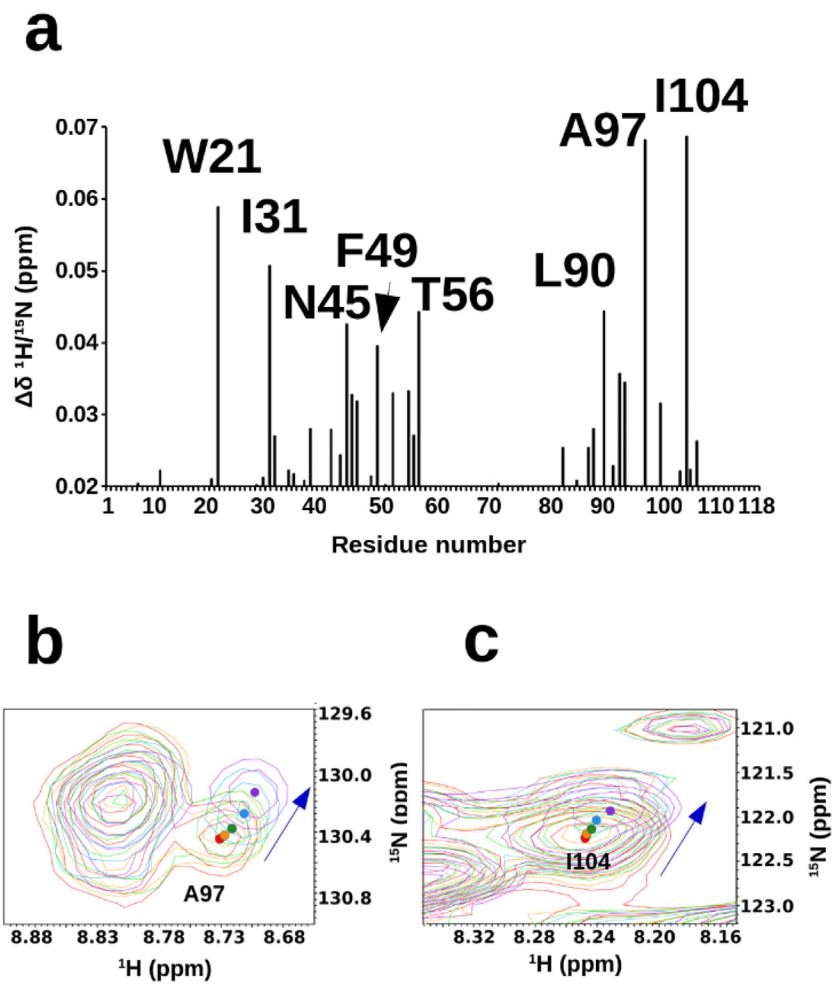

Fig. 3. ATP-rhNGF interactions by NMR titration. (a) – Map of combined $^{1}H/^{15}N$ CSP ($\Delta\delta$) of the HN groups of rhNGF upon binding of ATP. Only values above the threshold of 0.02 ppm are shown, based on the overall shift variation due ligand's addition. Residues with largest CSP ($\Delta\delta \geq 0.04$ ppm) are labelled. The combined $^{1}H/^{15}N$ CSP ($\Delta\delta$) were calculated from ^{1}H and ^{15}N CSP using the equation: $\Delta\delta = ((\Delta\delta\ ^{1}H)^2 + (0.04 \times \Delta\delta\ ^{15}N)^2)^{1/2}$ [50]. (b, c) – Expanded regions of 2D ^{1}H-^{15}N HSQC spectra showing a larger shift of A97 (b) and I104 (c) during titration (Colors for different ATP:rhNGF ratios: Red: 0 eq; Orange: 5 eq; Green: 10 eq; Cyan: 15 eq; Violet: 20 eq). (For interpretation of the references to colour in this figure legend, the reader is referred to the web version of this article.)

Table 1
Observations in the 3D ^{15}N-NOESY-HSQC spectrum collected at ATP-rhNGF titration endpoint indicating ATP binding to two sites.

	Site 1	Site 2
New NOEs between HN of rhNGF and ATP protons	V20 HN – ATP H2 E55 HN – ATP H2	F49 HN - ATP H3′
Changes in NOE patterns of rhNGF	V20, W21, V22, E55	Loop I (T29-K34) Loop II (S47, V48)

the NOE and CSP analysis. As clearly visible in Fig. 4 (a), ATP binding Site 1 partially overlaps with the binding cleft of rhNGF in the TrkA-d5 domain complex (PDB: 1WWW, 2IFG). Site 2 (Fig. 3(b)) nicely overlaps instead with the rhNGF binding site in the complex with extracellular domain of the $p75^{NTR}$ receptor (PDB: 1SG1). Two representative poses for the two sites are shown in Fig. 4 (c, d). In both poses, the distances between HN protons of residues of rhNGF engaged with ATP protons are shorter than 5 Å, in agreement with the identified NOE. These poses also well agree with the STD NMR experiments, showing an involvement of both adenine and sugar moieties of ATP in the rhNGF interaction (Supp. Fig. S7).

To further support the direct ATP-rhNGF interactions, based on our NMR approach and MD simulations, the potential energy differences (only the enthalpic term has been taken into account) were calculated, with respect to the unbound state, for the ATP-rhNGF interactions. These values are −14.6 ± 1.2 kcal/mol for Site 1 and −2.34 ± 1.3 kcal/mol for Site 2.

3.4. ATP-rhNGF binding: Effects on TrkA and $p75^{NTR}$ receptors

SPR data on ATP-rhNGF binding to TrkA and $p75^{NTR}$ receptors are in line with our NMR studies. We investigated ATP binding to the two receptors alone, as well as in the presence of divalent ions, namely Mg^{2+} (physiologically relevant) and Zn^{2+} (dysregulated in pathological conditions). The kinetics and affinity data highlight that ATP-Mg^{2+} weakly affect TrkA or $p75^{NTR}$ affinity if compared to rhNGF alone (Table 2, Supp. Fig. S11). In the case of ATP-Zn^{2+}, there is a clear decrease in the affinity *versus* the TrkA receptor, mediated by either Zn^{2+} alone or ATP-Zn^{2+}, as compared to rhNGF alone (Table 2, Supp. Fig. S11). The latter effect is less marked for the $p75^{NTR}$ receptor (Table 2, Supp. Fig. S11).

These effect clearly depend on the relative stoichiometry of the ATP-ion-rhNGF mixture. By careful comparison of the response level for the ATP-ion-rhNGF samples with the reference rhNGF, it emerges that the different ligands induce a change in the maximum response level, on either receptor. This might indicate a change in the fraction of the analyte binding to the receptors. Since

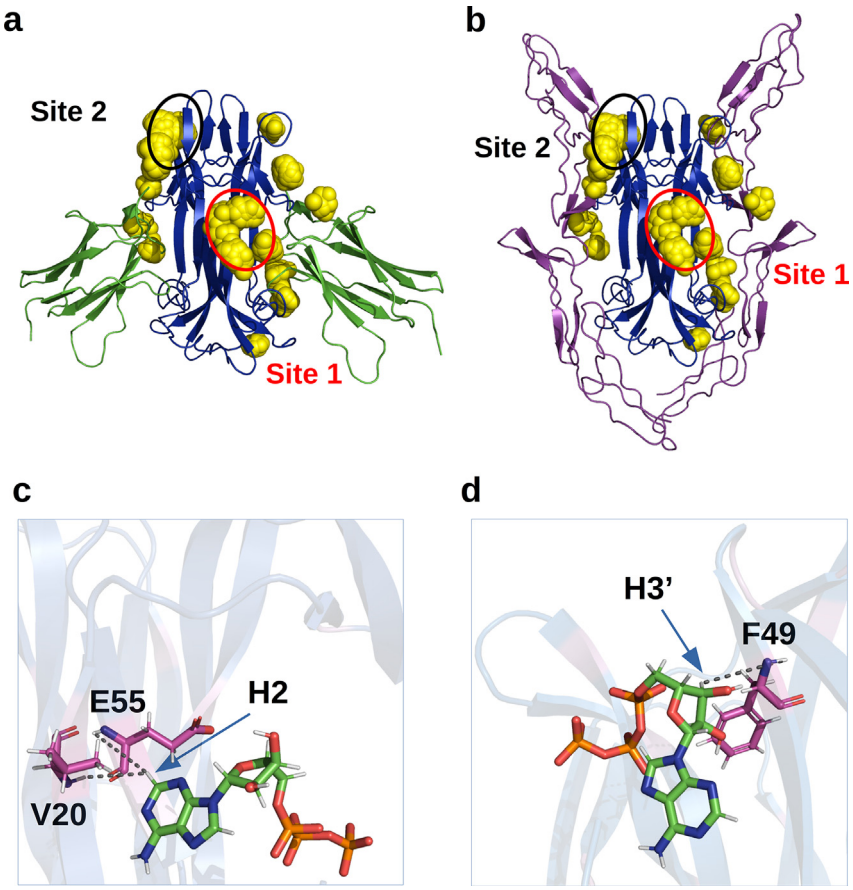

Fig. 4. Binding orientation of ATP on rhNGF. (a, b) – Representation of the most frequently occupied regions for ATP onto rhNGF, according to the MD simulations (yellow spheres clusters). Sites 1 and 2 are indicated by red and black circles, respectively. Superposition of the clusters on rhNGF (blue) and the TrkA-d5 domain (green, PDB: 1WWW) (a) and $p75^{NTR}$ extracellular domain (magenta, PDB: 1SG1) (b). (c, d) – Representative poses from MD analysis for Site 1 (c) and Site 2 (d). Cartoon transparent blue: rhNGF; cartoon transparent purple: residues with larger CSP; ATP is represented as colored by element (C – green; N – blue; O – red; H – white; P – orange). Residues V20, E55 and F49 showing new NOEs upon ATP binding are labelled and colored by element (C – magenta; N – blue; O – red; H – white). The distances between HN protons of rhNGF and ATP protons (indicated by a blue arrow) are represented by black broken lines. Figures produced using PyMOL [58]. (For interpretation of the references to colour in this figure legend, the reader is referred to the web version of this article.)

Table 2
Summary of the affinity data obtained for the kinetic analysis of the different combinations of rhNGF *plus* divalent ion and/or ATP. For each receptor, the values for the affinity constant (K_D) are reported, together with the standard deviation.

Sample	TrkA K_D (nM)	$p75^{NTR}$ K_D (nM)
rhNGF	0.16	0.83
Mg^{2+}-rhNGF	0.30 ± 0.14	0.99 ± 0.32
ATP-Mg^{2+}-rhNGF	0.31 ± 0.09	1.02 ± 0.23
Zn^{2+}-rhNGF	0.49 ± 0.18	1.04 ± 0.18
ATP-Zn^{2+}-rhNGF	0.69 ± 0.12	1.43 ± 0.7

ATP binds with low affinity to rhNGF, this is an indirect evidence of the formation of the ATP-ion-rhNGF complex, which transiently forms during the SPR experiment in small percentage. This effect is stoichiometry-dependent (ATP-ion-rhNGF) and differs when considering Mg^{2+} or Zn^{2+} (Supp. Fig. S12). In the case of a large excess of Zn^{2+} and ATP a dramatic change in the curve shape is observed, reflecting a change in the binding mode. This is not surprising, having been early reported that Zn^{2+} binds to NGF [67] . To investigate the active role of the ions in the ATP-rhNGF receptors' interaction, a qualitatively control experiment was carried out by pre-incubating the ATP-ion-rhNGF prior to SPR injection. In the case of Mg^{2+}, no effect of the pre-mixing was observed on the binding affinity (TrkA (K_D = 0.27 nM); $p75^{NTR}$ (K_D = 1.07 nM) with respect to rhNGF alone (TrkA K_D = 0.16 nM; $p75^{NTR}$ K_D = 0.83 nM). The preincubated ATP-Zn^{2+}-rhNGF mixture resulted in a clear trend towards a decrease of the affinity to either TrkA (K_D = 0.89 nM) or $p75^{NTR}$ (K_D = 3.20 nM) with respect to rhNGF alone (TrkA K_D = 0.16 nM; $p75^{NTR}$ K_D = 0.83 nM) and confirmed a more pronounced effect on TrkA than on $p75^{NTR}$ receptor's binding.

4. Discussion

The present study by integrative structural biology, combining multiple experimental techniques, unveiled the binding cartography of ATP to rhNGF, aiming at the structural and functional characterization of new endogenous modulators of NGF biological activity.

The ATP-rhNGF binding is characterized by low affinity (mM range), as confirmed by SPR, ITC and STD-NMR. It can thus be counted among transient interactions with weak affinities, named "quinary interactions", which were recently highlighted [61] to be important for the regulation of dynamic biological processes needed for cell survival. Therefore, our data prompt to ATP as a modulator of neurotrophins activity.

Many biological data confirmed the presence of low extracellular ATP levels in physiological conditions, while increased extracellular ATP levels up to mM concentration have been reported to cause cell damage or inflammation. The ATP modulating purinergic signaling suggests that any alteration of the fine tuning may affect several human diseases, including neurodegenerative disorders as

well as inflammatory dysfunction and tumors [33]. High levels of Zn^{2+} were found in cell damage or neurodegenerative conditions [28]. What is more, ATP in the 0.1–10 mM concentration range have been recently reported to kinetically modulate pathogenic tau fibrillation [68]. Furthermore, millimolar concentrations of ATP were found to be linked to a reduction of the fibrillation of neuronal proteins [69] and ATP was found to specifically bind the RNA-binding domain of the nucleocapsid protein of SARS-CoV-2 with a millimolar K_D [70].

We investigated the concomitant presence of ATP and Mg^{2+} or Zn^{2+} and conclude that a tight regulation of the relative stoichiometry of ATP-ion-rhNGF is needed to modulate the endogenous biological response. Indeed, it is well established that NTs and the purinergic receptors systems are in functional interplay, in physiological as well as in pathological conditions [71,72]. The direct ATP and rhNGF interaction was however only recently described [20]. Our data support this finding. Based on the solution NMR titration of ATP to rhNGF we identified the residues in contact with ATP, localized in Loops I, II and V. The solution NMR analysis in the presence of Mg^{2+} allowed identifying new NOEs attributable to ATP, which pointed to the existence of two binding sites of ATP on rhNGF, identified as Site 1 and Site 2. These data were functionally used to guide an MD study to map the likely orientation of ATP in binding the rhNGF. Site 1 cover regions involved into the binding of rhNGF to the TrkA-d5 domain, while residues involved in the Site 2 belong instead to the region of rhNGF known to be involved into the binding with $p75^{NTR}$ receptor extracellular domain.

It is worthy of mention that König et al. [21] suggested one of the two ATP-binding sites to be located close to the cysteine knot in rhNGF. Furthermore, time-dependent proteolytic digestion followed by EI and MALDI-TOF MS analyses prompted to the stability of the ATP-rhNGF complex to be unaffected by the loss of the N-terminal (1–9) peptide SSSHPIFHR and of the Loop II (35–50) peptide EVMVLG EVNINNSVFK. As depicted in Fig. 5, our combined CSP NMR data and MD simulations weakly support these findings.

Based on MS experiments, Rose et al. [73] prompted ATP binding site of the FGF2 growth factor to overlap with its HBD. Moreover, it has been previously hypothesized that NGF also possesses a HBD (amino acids 113–120) that binds heparin very weakly [74]. Since evidences have been provided, that residues (113–115) within the HBD play an important role for bioactivity of NGF [75] Hasche et al. [22] exploited several rhNGF mutants. They tested whether the mutant proteins could still bind to ATP as well as whether the ATP-rhNGF conjugates could still act as neuroprotective ligands. Interestingly all mutants (rhNGF(K115S) and rhNGF(S113T/R114S/K115S)) but one (rhNGF(L112A)) lost their ability to bind ATP as well as their ATP mediated neuroprotection. It is tempting to hypothesize that the loss of ATP binding and neuroprotective activity could likely be ascribed to misfolding of the rhNGF mutants, as being already suggested for rhNGF mutants at these very same positions reported to have lost their bioactivity in several bioassays (PC12 cells neurite outgrowth, TrkA phosphorylation and binding) [75]. It is worthy of note that none of the above-mentioned rhNGF mutants, located at the C-termnus of rhNGF and proposed to be part of the rhNGF HBD, overlap with the residues encompassing either of the two ATP-rhNGF binding sites unveiled in the present study. In addition, the proposed C-terminal residues of rhNGF do not overlap either with those rhNGF residues, elucidated by using carbohydrate microarray and computational approaches, to be involved instead in interactions with glycosaminoglycans [18]. Intriguingly, one of the two ATP-rhNGF binding sites unveiled in the present study, namely Site 2, instead, fully overlap with that proposed by Rogers et al. [18] for the CS-E, a glycosaminoglycan homolog of heparin, to bind to rhNGF (Fig. 5).

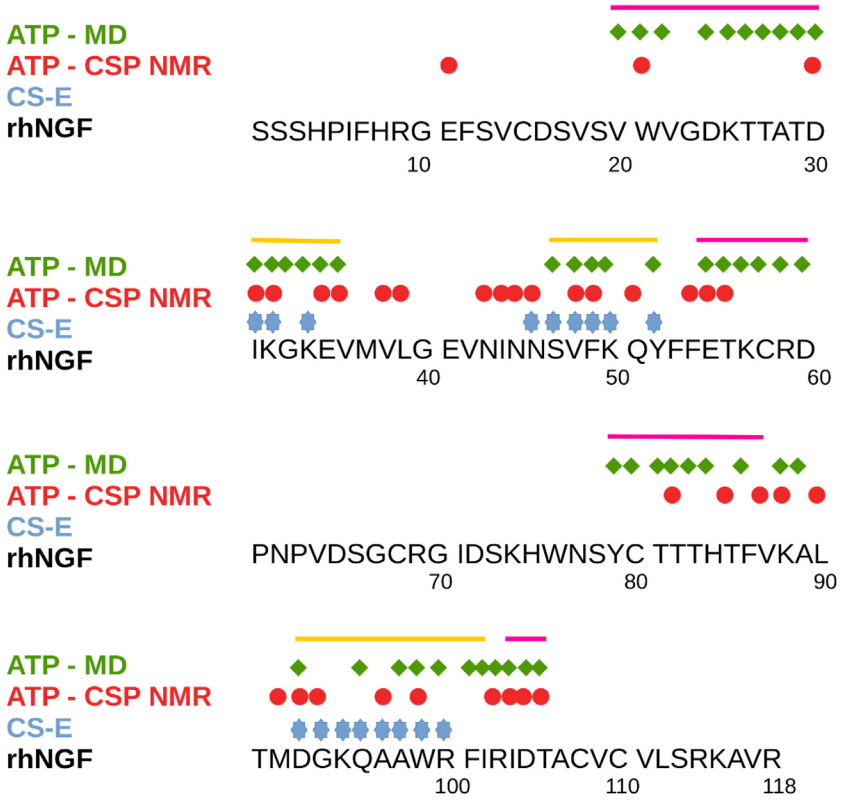

Fig. 5. rhNGF ligands binding sites. rhNGF residues in contacts with ATP during MD simulations (green filled diamonds). rhNGF residues affected in NMR CSP upon ATP titration (red filled circle). rhNGF residues predicted by computational docking [18] to be involved (within 5 Å of the oligosaccharide) in CS-E binding (light blue filled "stars"); rhNGF residues within 5 Å from ATP binding Site 1 or Site 2 according to the best MD poses (see Fig. 4) are highlighted by magenta or yellow upper lines, respectively. (For interpretation of the references to colour in this figure legend, the reader is referred to the web version of this article.)

Furthermore, the binding of lipids to NGF have been shown to possibly result in shifting the equilibrium between forming the NGF-$p75^{NTR}$ complex or forming the NGF-TrkA complex thus shaping the signal transduction pattern of NGF. Interestingly crystallographic studies of mouse and cobra NGF-lipids complexes indicated that lysophosphatidyl serine (PDB ID 4EAX), lysophosphatidylinositol (PDB ID 4XPJ) and docosanoic (PDB ID 4EC7) acid all bind in a NGF pocket-lining residues mostly overlapping Site 2 [17,59].

Thus, our findings clearly highlight Site 1 as a likely specific ATP-rhNGF binding site, whereas Site 2 represents a likely promiscuous rhNGF binding site for endogenous ligands such as ATP, glycosaminoglycans and lipids. Indeed, this hypothesis is substantiated by the significantly difference in the potential energy of NGF-ATP interactions of Site1 *versus* Site2. The relative binding enthalpy of ATP for Site 1 is indeed −12.2 kcal/mol lower than for Site 2. This observation opens new potential investigational avenues for the biological implication of these small molecules binding into NTs biology.

The present results further support the suggested role of ATP as a functional endogenous modulator of NGF bioactivity. SPR data on rhNGF binding to the TrkA and $p75^{NTR}$ receptors well agree with our NMR studies. The K_D affinity values of rhNGF binding to its receptors showed a weak effect of either Mg^{2+} or ATP-Mg^{2+}. In the presence of Zn^{2+} or ATP-Zn^{2+} we detected a higher effect (lower rhNGF binding affinity) on TrkA than on the $p75^{NTR}$ receptor. This clearly depends on the relative stoichiometry of the ATP-ion-rhNGF mixture and is more evident in the presence of a large excess of ATP-Zn^{2+}.

As demonstrated previously by MALDI-TOF MS analysis, the stoichiometry of the ATP-rhNGF complex depends on the type of divalent ions [21,22]. It is tempting to hypothesize that in physiological conditions, ATP might amplify hNGF signaling through TrkA receptor, as reported [23]. In neurodegeneration or cellular stress, massive release of extracellular ATP is reported [33] while a reduction of TrkA signaling has been observed [76]. In line with this, our data suggest a reduction of hNGF affinity for the TrkA receptor in the presence of Zn^{2+} and ATP. Moreover, the activation of P2X receptors by mM ATP concentration in trauma conditions triggers the prevention of a large inflammatory response [32,71]. The direct binding of ATP to hNGF – albeit of low affinity - might also serve as a molecular switch for the relative activation of NTs *versus* purinergic receptors systems to meet better the cellular needs.

5. Conclusion

The present 3D binding cartography and the functional description of the ATP-rhNGF interaction represents an important step towards the understanding of the complex puzzle underlying the molecular determinants of NTs binding to its receptors in health and disease. Furthermore, it paves the way towards to the characterization of other multifunctional endogenous ligands (*e.g.* lipids, lysophospholipids, fatty acids and glycosaminoglycan oligosaccharides [15,18,19]) as novel transient modulators of NGF, as well as of the other members of the NT family [77]. The outcomes of the present structural study shall pave the way for further extending the research on this important biological topic aiming at the precise identification of the molecular mechanism underlying neurotrophins signaling by endogenous small molecules and the cross-talk with the purinergic pathways.

CRediT authorship contribution statement

Francesca Paoletti: Conceptualization, Formal analysis, Investigation, Writing, Visualization. **Franci Merzel:** Formal analysis, Investigation, Visualization, Funding acquisition. **Alberto Cassetta:** Formal analysis, Investigation, Visualization. **Iza Ogris:** Formal analysis, Investigation. **Sonia Covaceuszach:** Formal analysis, Investigation, Visualization. **Jože Grdadolnik:** Formal analysis, Investigation, Visualization, Funding acquisition. **Doriano Lamba:** Conceptualization, Formal analysis, Investigation, Writing, Visualization. **Simona Golič Grdadolnik:** Conceptualization, Formal analysis, Investigation, Writing, Visualization, Funding acquisition.

Declaration of Competing Interest

The authors declare that they have no known competing financial interests or personal relationships that could have appeared to influence the work reported in this paper.

Acknowledgments

This work was supported by Slovenian Research Agency (Grant No. J1-8145, P1-0010 and J1-1705). We recorded NMR spectra on NMR spectrometers of Slovenian NMR Centre at National Institute of Chemistry. We acknowledge the skillful assistance of Gregor Bajc (Infrastructural Centre for Analysis of Molecular Interactions, Ljubljana) for the recording of SPR data. We acknowledge Dr. David Pahovnik and Dr. Ema Žagar (Department of Polymer Chemistry and Technology, National Institute of Chemistry) for acquiring the MALDI-MS spectra on rhNGF. We thank Dr. Francesca Malerba and Prof. Antonino Cattaneo (European Brain Research Institute - EBRI, Roma, Italy) for the generous gift of the pET11a plasmid containing the cDNA of human proNGF VSAR.

Appendix A. Supplementary data

Supplementary data to this article can be found online at https://doi.org/10.1016/j.csbj.2021.05.009.

References

[1] Levi-Montalcini R. The nerve growth factor 35 years later. Science 1987;237 (4819):1154–62.
[2] Hefti FF, Rosenthal A, Walicke PA, Wyatt S, Vergara G, Shelton DL, et al. Novel class of pain drugs based on antagonism of NGF. Trends Pharmacol Sci 2006;27 (2):85–91. https://doi.org/10.1016/j.tips.2005.12.001.
[3] Lee R, Kermani P, Teng KK, Hempstead BL. Regulation of cell survival by secreted proneurotrophins. Science 2001;294:1945–8. https://doi.org/10.1126/science.1065057.
[4] Ivanisevic L, Banerjee K, Saragovi HU. Differential cross-regulation of TrkA and TrkC tyrosine kinase receptors with p75. Oncogene 2003;22(36):5677–85. https://doi.org/10.1038/sj.onc.1206864.
[5] Zaccaro MC, Ivanisevic L, Perez P, Meakin SO, Saragovi HU. p75 Co-receptors regulate ligand-dependent and ligand-independent Trk receptor activation, in part by altering Trk docking subdomains. J Biol Chem 2001;276(33):31023–9. https://doi.org/10.1074/jbc.M104630200.
[6] Nykjaer A, Lee R, Teng KK, Jansen P, Madsen P, Nielsen MS, et al. Sortilin is essential for proNGF-induced neuronal cell death. Nature 2004;427 (6977):843–8. https://doi.org/10.1038/nature02319.
[7] Allen SJ, Dawbarn D. Clinical relevance of the neurotrophins and their receptors. Clin Sci 2006;110:175–91. https://doi.org/10.1042/CS20050161.
[8] Longo FM, Massa SM. Small-molecule modulation of neurotrophin receptors: a strategy for the treatment of neurological disease. Nat Rev Drug Discov 2013;12(7):507–25. https://doi.org/10.1038/nrd4024.
[9] Hirose M, Kuroda Y, Murata E. NGF/TrkA signaling as a therapeutic target for pain. Pain Pract 2016;16(2):175–82. https://doi.org/10.1111/papr.12342.
[10] Kennedy AE, Laamanen CA, Ross MS, Vohra R, Boreham DR, Scott JA, et al. Nerve growth factor inhibitor with novel-binding domain demonstrates nanomolar efficacy in both cell-based and cell-free assay systems. Pharmacol Res Perspect 2017;5(5):e00339. https://doi.org/10.1002/prp2.339.
[11] Moosavi F, Hosseini R, Saso L, Firuzi O. Modulation of neurotrophic signaling pathways by polyphenols. Drug Des Devel Ther 2016;10:23–42. https://doi.org/10.2147/DDDT.S96936.
[12] Venkatesan R, Ji E, Kim SY. Phytochemicals that regulate neurodegenerative disease by targeting neurotrophins: a comprehensive review. Biomed Res Int 2015;2015:1–22. https://doi.org/10.1155/2015/814068.
[13] Niederhauser O, Mangold M, Schubenel R, Kusznir EA, Schmidt D, Hertel C. NGF ligand alters NGF signaling via p75(NTR) and trkA. J Neurosci Res

2000;61:263–72. https://doi.org/10.1002/1097-4547(20000801)61:3<263::AID-JNR4>3.0.CO;2-M.
[14] Jarvis T, Davies D, Hisaminato A, Resnicow D, Gupta S, Waugh S, et al. Non-helical DNA triplex forms a unique aptamer scaffold for high affinity recognition of nerve growth factor. Structure 2015;23(7):1293–304. https://doi.org/10.1016/j.str.2015.03.027.
[15] Lourenssen S, Blennerhassett MG. Lysophosphatidylserine potentiates nerve growth factor-induced differentiation of PC12 cells. Neurosci Lett 1998;248(2):77–80.
[16] Kawamoto K, Aoki J, Tanaka A, Itakura A, Hosono H, Arai H, et al. Nerve growth factor activates mast cells through the collaborative interaction with lysophosphatidylserine expressed on the membrane surface of activated platelets. J Immunol 2002;168(12):6412–9.
[17] Tong Q, Wang F, Zhou H-Z, Sun H-L, Song H, Shu Y-Y, et al. Structural and functional insights into lipid-bound nerve growth factors. FASEB J 2012;26(9):3811–21. https://doi.org/10.1096/fsb2.v26.910.1096/fj.12-207316.
[18] Rogers CJ, Clark PM, Tully SE, Abrol R, Garcia KC, Goddard WA, et al. Elucidating glycosaminoglycan-protein-protein interactions using carbohydrate microarray and computational approaches. Proc Natl Acad Sci USA 2011;108(24):9747–52. https://doi.org/10.1073/pnas.1102962108.
[19] Liu P, Chen L, Toh JKC, Ang YL, Jee J-E, Lim J, et al. Tailored chondroitin sulfate glycomimetics via a tunable multivalent scaffold for potentiating NGF/TrkA-induced neurogenesis. Chem Sci 2015;6(1):450–6. https://doi.org/10.1039/C4SC02553A.
[20] Klumpp S, Kriha D, Bechmann G, Maaßen A, Maier S, Pallast S, et al. Phosphorylation of the growth factors bFGF, NGF and BDNF: a prerequisite for their biological activity. Neurochem Int 2006;48(2):131–7. https://doi.org/10.1016/j.neuint.2005.08.009.
[21] König S, Hasche A, Pallast S, Krieglstein J, Klumpp S. Detection of ATP-binding to growth factors. J Am Soc Mass Spectrom 2008;19(1):91–5. https://doi.org/10.1016/j.jasms.2007.10.010.
[22] Hasche A, Ferenz KB, Rose K, König S, Humpf H-U, Klumpp S, et al. Binding of ATP to nerve growth factor: characterization and relevance for bioactivity. Neurochem Int 2010;56(2):276–84. https://doi.org/10.1016/j.neuint.2009.10.012.
[23] Ferenz KB, Rose K, König S, Krieglstein J. ATP-NGF-complex, but not NGF, is the neuroprotective ligand. Neurochem Int 2011;59(7):989–95. https://doi.org/10.1016/j.neuint.2011.08.020.
[24] Ferenz KB, Gast RE, Rose K, Finger IE, Hasche A, Krieglstein J. Nerve growth factor and brain-derived neurotrophic factor but not granulocyte colony-stimulating factor, nimodipine and dizocilpine, require ATP for neuroprotective activity after oxygen-glucose deprivation of primary neurons. Brain Res 2012;1448:20–6. https://doi.org/10.1016/j.brainres.2012.02.016.
[25] Rose K. Interaction of ATP with fibroblast growth factor 2: biochemical characterization and consequence for growth factor stability. BMC Biochem 2011;12(1):14. https://doi.org/10.1186/1471-2091-12-14.
[26] Gast RE, König S, Rose K, Ferenz KB, Krieglstein J. Binding of ATP to vascular endothelial growth factor isoform VEGF-A165 is essential for inducing proliferation of human umbilical vein endothelial cells. BMC Biochem 2011;12(1):28. https://doi.org/10.1186/1471-2091-12-28.
[27] Granzotto A, Sensi SL. Intracellular zinc is a critical intermediate in the excitotoxic cascade. Neurobiol Dis 2015;81:25–37. https://doi.org/10.1016/j.nbd.2015.04.010.
[28] Morris DR, Levenson CW. Ion channels and zinc: mechanisms of neurotoxicity and neurodegeneration. J Toxicol 2012;2012:1–6. https://doi.org/10.1155/2012/785647.
[29] Pochwat B, Nowak G, Szewczyk B. Relationship between Zinc (Zn (2+)) and Glutamate Receptors in the Processes Underlying Neurodegeneration. Neural Plast 2015;2015:. https://doi.org/10.1155/2015/591563591563.
[30] Sánchez-Martín FJ, Valera E, Casimiro I, Merino JM. Nerve growth factor increases the sensitivity to zinc toxicity and induces cell cycle arrest in PC12 cells. Brain Res Bull 2010;81(4-5):458–66. https://doi.org/10.1016/j.brainresbull.2009.11.008.
[31] Morley SN, Power JM, Coulson EJ, Bartlett PF. Zinc-mediated neuronal death is dependent on Trk activation. Exp Neurol 2007;205(2):360–6. https://doi.org/10.1016/j.expneurol.2007.02.006.
[32] Burnstock G. An introduction to the roles of purinergic signalling in neurodegeneration, neuroprotection and neuroregeneration. Neuropharmacology 2016;104:4–17. https://doi.org/10.1016/j.neuropharm.2015.05.031.
[33] Volonté C, Amadio S, Cavaliere F, D'Ambrosi N, Vacca F, Bernardi G. Extracellular ATP and neurodegeneration. Curr Drug Targets CNS Neurol Disord 2003;2:403–12. https://doi.org/10.2174/1568007033482643.
[34] Cavaliere F, Sancesario G, Bernardi G, Volonté C. Extracellular ATP and nerve growth factor intensify hypoglycemia-induced cell death in primary neurons: role of P2 and NGFRp75 receptors. J Neurochem 2002;83:1129–38. https://doi.org/10.1046/j.1471-4159.2002.01205.x.
[35] D'Ambrosi N, Murra B, Cavaliere F, Amadio S, Bernardi G, Burnstock G, et al. Interaction between ATP and nerve growth factor signalling in the survival and neuritic outgrowth from PC12 cells. Neuroscience 2001;108(3):527–34. https://doi.org/10.1016/S0306-4522(01)00431-6.
[36] Shuker SB, Hajduk PJ, Meadows RP, Fesik SW. Discovering high-affinity ligands for proteins: SAR by NMR. Science 1996;274(5292):1531–4.
[37] Horst R, Farley KA, Kormos BL, Withka JM. NMR spectroscopy: the swiss army knife of drug discovery. J Biomol NMR 2020;74(10-11):509–19. https://doi.org/10.1007/s10858-020-00330-0.
[38] Hanzawa H, Shimada T, Takahashi M, Takahashi H. Revisiting biomolecular NMR spectroscopy for promoting small-molecule drug discovery. J Biomol NMR 2020;74(10-11):501–8. https://doi.org/10.1007/s10858-020-00314-0.
[39] Erlanson DA, Davis BJ, Jahnke W. Fragment-based drug discovery: advancing fragments in the absence of crystal structures. Cell Chemical Biology 2019;26(1):9–15. https://doi.org/10.1016/j.chembiol.2018.10.001.
[40] Rattenholl A, Lilie H, Grossmann A, Stern A, Schwarz E, Rudolph R. The pro-sequence facilitates folding of human nerve growth factor from Escherichia coli inclusion bodies. Eur J Biochem 2001;268:3296–303.
[41] Paoletti F, de Chiara C, Kelly G, Covaceuszach S, Malerba F, Yan R, et al. Conformational rigidity within plasticity promotes differential target recognition of nerve growth factor. Front Mol Biosci 2016;3. https://doi.org/10.3389/fmolb.2016.00083.
[42] Muhandiram DR, Kay LE. Gradient-enhanced triple-resonance three-dimensional nmr experiments with improved sensitivity. J Magn Reson, Ser B 1994;103(3):203–16. https://doi.org/10.1006/jmrb.1994.1032.
[43] Delaglio F, Grzesiek S, Vuister GW, Zhu G, Pfeifer J, Bax A. NMRPipe: a multidimensional spectral processing system based on UNIX pipes. J Biomol NMR 1995;6:277–93.
[44] Keller R. The Computer Aided Resonance Assignment Tutorial. First edition. 2004.
[45] Rieping W, Habeck M, Bardiaux B, Bernard A, Malliavin TE, Nilges M. ARIA2: automated NOE assignment and data integration in NMR structure calculation. Bioinformatics 2007;23(3):381–2. https://doi.org/10.1093/bioinformatics/btl589.
[46] Mareuil F, Malliavin TE, Nilges M, Bardiaux B. Improved reliability, accuracy and quality in automated NMR structure calculation with ARIA. J Biomol NMR 2015;62(4):425–38. https://doi.org/10.1007/s10858-015-9928-5.
[47] Mayer M, Meyer B. Group epitope mapping by saturation transfer difference NMR to identify segments of a ligand in direct contact with a protein receptor. J Am Chem Soc 2001;123(25):6108–17. https://doi.org/10.1021/ja0100120.
[48] Yan J, Kline AD, Mo H, Shapiro MJ, Zartler ER. The effect of relaxation on the epitope mapping by saturation transfer difference NMR. J Magn Reson 2003;163(2):270–6. https://doi.org/10.1016/S1090-7807(03)00106-X.
[49] McCullough C, Wang M, Rong L, Caffrey M. Characterization of influenza hemagglutinin interactions with receptor by NMR. PLoS ONE 2012;7(7):e33958. https://doi.org/10.1371/journal.pone.0033958.
[50] Hajduk PJ, Meadows RP, Fesik SW. Discovering high-affinity ligands for proteins. Science 1997;278(497):499. https://doi.org/10.1126/science.278.5337.497.
[51] Ericsson UB, Hallberg BM, DeTitta GT, Dekker N, Nordlund P. Thermofluor-based high-throughput stability optimization of proteins for structural studies. Anal Biochem 2006;357(2):289–98. https://doi.org/10.1016/j.ab.2006.07.027.
[52] Keller S, Vargas C, Zhao H, Piszczek G, Brautigam CA, Schuck P. High-precision isothermal titration calorimetry with automated peak-shape analysis. Anal Chem 2012;84(11):5066–73. https://doi.org/10.1021/ac3007522.
[53] Zhao H, Piszczek G, Schuck P. SEDPHAT–a platform for global ITC analysis and global multi-method analysis of molecular interactions. Methods 2015;76:137–48. https://doi.org/10.1016/j.ymeth.2014.11.012.
[54] Phillips JC, Braun R, Wang W, Gumbart J, Tajkhorshid E, Villa E, et al. Scalable molecular dynamics with NAMD. J Comput Chem 2005;26(16):1781–802. https://doi.org/10.1002/jcc.v26:1610.1002/jcc.20289.
[55] Brooks BR, Brooks CL, Mackerell AD, Nilsson L, Petrella RJ, Roux B, et al. CHARMM: the biomolecular simulation program. J Comput Chem 2009;30(10):1545–614. https://doi.org/10.1002/jcc.v30:1010.1002/jcc.21287.
[56] Paoletti F, Covaceuszach S, Konarev PV, Gonfloni S, Malerba F, Schwarz E, et al. Intrinsic structural disorder of mouse proNGF. Proteins 2009;75(4):990–1009. https://doi.org/10.1002/prot.v75:410.1002/prot.22311.
[57] McDonald NQ, Lapatto R, Murray-Rust J, Gunning J, Wlodawer A, Blundell TL. New protein fold revealed by a 2.3-A resolution crystal structure of nerve growth factor. Nature 1991;354:411–4. https://doi.org/10.1038/354411a0.
[58] The PyMOL Molecular Graphics System, Version 2.0. Schrödinger, LLC
[59] Sun HL, Jiang T. The structure of nerve growth factor in complex with lysophosphatidylinositol. Acta Crystallogr F Struct Biol Commun 2015;71:906–12. https://doi.org/10.1107/S2053230X15008870.
[60] Paoletti F, Malerba F, Bruni Ercole B, Lamba D, Cattaneo A. A comparative analysis of the structural, functional and biological differences between Mouse and Human Nerve Growth Factor. Biochim Biophys Acta 2015;1854(3):187–97. https://doi.org/10.1016/j.bbapap.2014.12.005.
[61] McConkey EH. Molecular evolution, intracellular organization, and the quinary structure of proteins. Proc Natl Acad Sci USA 1982;79(10):3236–40. https://doi.org/10.1073/pnas.79.10.3236.
[62] Qin J, Gronenborn AM. Weak protein complexes: challenging to study but essential for life. FEBS J 2014;281(8):1948–9. https://doi.org/10.1111/febs.12744.
[63] Chien P, Gierasch LM, Kozminski KG, Lippincott-Schwartz J. Challenges and dreams: physics of weak interactions essential to life. Mol Biol Cell 2014;25(22):3474–7. https://doi.org/10.1091/mbc.e14-06-1035.
[64] Sukenik S, Ren P, Gruebele M. Weak protein-protein interactions in live cells are quantified by cell-volume modulation. Proc Natl Acad Sci USA 2017;114:6776–81. https://doi.org/10.1073/pnas.1700818114.

[65] Luna RE, Akabayov SR, Ziarek JJ, Wagner G. Examining weak protein-protein interactions in start codon recognition via NMR spectroscopy. FEBS J 2014;281(8):1965–73. https://doi.org/10.1111/febs.12667.
[66] Cohen RD, Pielak GJ. A cell is more than the sum of its (dilute) parts: a brief history of quinary structure. Protein Sci 2017;26(3):403–13. https://doi.org/10.1002/pro.3092.
[67] Maitra R, Shamovsky IL, Wang W, Solc M, Lawrance G, Dostaler SM, et al. Differential effects of transition metal cations on the conformation and biological activities of nerve growth factor. Neurotox Res 2000;2(4):321–41. https://doi.org/10.1007/BF03033341.
[68] Heo CE, Han JY, Lim S, Lee J, Im D, Lee MJ, et al. ATP Kinetically Modulates Pathogenic Tau Fibrillations. ACS Chem Neurosci 2020;11(19):3144–52. https://doi.org/10.1021/acschemneuro.0c0047910.1021/acschemneuro.0c00479.s001.
[69] Kang J, Lim L, Song J. ATP binds and inhibits the neurodegeneration-associated fibrillization of the FUS RRM domain. Commun Biol 2019;2:1–10. https://doi.org/10.1038/s42003-019-0463-x.
[70] Dang M, Li Y, Song J. ATP biphasically modulates LLPS of SARS-CoV-2 nucleocapsid protein and specifically binds its RNA-binding domain. Biochem Biophys Res Commun 2021;541:50–5. https://doi.org/10.1016/j.bbrc.2021.01.018.
[71] Woods LT, Ajit D, Camden JM, Erb L, Weisman GA. Purinergic receptors as potential therapeutic targets in Alzheimer's disease. Neuropharmacology 2016;104:169–79. https://doi.org/10.1016/j.neuropharm.2015.10.031.
[72] Arthur DB, Akassoglou K, Insel PA. P2Y2 receptor activates nerve growth factor/TrkA signaling to enhance neuronal differentiation. Proc Natl Acad Sci USA 2005;102(52):19138–43. https://doi.org/10.1073/pnas.0505913102.
[73] Rose K, Pallast S, Klumpp S, Krieglstein J. ATP-binding on fibroblast growth factor 2 partially overlaps with the heparin-binding domain. J Biochem 2008;144:343–7. https://doi.org/10.1093/jb/mvn072.
[74] Sakiyama-Elbert SE, Hubbell JA. Controlled release of nerve growth factor from a heparin-containing fibrin-based cell ingrowth matrix. J Control Release 2000;69(1):149–58. https://doi.org/10.1016/S0168-3659(00)00296-0.
[75] Krüttgen A, Heymach JV, Kahle PJ, Shooter EM. The role of the nerve growth factor carboxyl terminus in receptor binding and conformational stability. J Biol Chem 1997;272(46):29222–8. https://doi.org/10.1074/jbc.272.46.29222.
[76] Counts SE, Mufson EJ. The role of nerve growth factor receptors in cholinergic basal forebrain degeneration in prodromal Alzheimer disease. J Neuropathol Exp Neurol 2005;64(4):263–72. https://doi.org/10.1093/jnen/64.4.263.
[77] Miras-Portugal MT, Gomez-Villafuertes R, Gualix J, Diaz-Hernandez JI, Artalejo AR, Ortega F, et al. Nucleotides in neuroregeneration and neuroprotection. Neuropharmacology 2016;104:243–54. https://doi.org/10.1016/j.neuropharm.2015.09.002.